The 9th European Congress on Computational Methods in Applied Sciences and Engineering
ECCOMAS Congress 2024
3 – 7 June 2024, Lisboa, Portugal

SOFTWARE IMPLEMENTATION TO SIMULATE THE HEMODYNAMICS IN PATIENT-SPECIFIC CORONARY ARTERIES: A REVIEW FROM THE PAST TO THE PRESENT

SÓNIA I.S. PINTO*

* Engineering Faculty of University of Porto (FEUP)
Department of Mechanical Engineering (DEMec)
Institute of Science and Innovation in Mechanical and Industrial Engineering (LAETA-INEGI)
Rua Dr. Roberto Frias 4200 – 465 Porto, Portugal
e-mail: spinto@fe.up.pt, https://orcid.org/0000-0002-2362-6538

Key words: Programming, Lumped-Parameter Model, Viscoelasticity, Coronary Arteries.

Summary. The present study is a review of the numerical implementation of the author and her research team for hemodynamic simulations in patient-specific coronary arteries. The author, as Professor of the Engineering Faculty of University of Porto (DEMec), has two lines of research since she is an Integrated Member of the Institute of Science and Innovation in Mechanical and Industrial Engineering (LAETA-INEGI). From 2018 to February 2021, the research centered on the correlation between the geometric parameters of patient-specific coronary arteries in the susceptibility of atherosclerosis formation, implementing the most accurate rheology of blood. Recently, after March 2021, the research is complemented focusing on the Fractional Flow Reserve (FFR) calculation using a non-invasive method. The main interest of the author to improve current diagnostic capabilities and enhancing patient care in the context of cardiovascular diseases. This is the aim of the ongoing project in collaboration with a Portuguese public hospital.

1 INTRODUCTION

Cardiovascular diseases (CAD) have been one of the main cause of mortality in advanced countries [1]. From clinical practice, it is well known that specific locations in the coronary tree are sensitive to develop atherosclerosis - the accumulation of lipoproteins inside the artery – causing a stenosis which blocks the normal circulation of blood flow.

Computed Tomography (CT) scans, provided by medical doctors of the hospital, can give information about the geometry of the coronary artery and the location of the atherosclerotic disease [1] but do not explain the hemodynamics in detail. Thus, numerical study of human blood flow has been an auxiliary tool for the prevention and treatment of CAD and has helping cardiologists to better manage such disease. However, modelling the hemodynamics with real physiological conditions of each patient, using principles of physics, mathematics and engineering, is still a challenge.

From 2018 to February 2021, the first goal was to study the correlation between the geometric parameters of patient-specific coronary arteries, such as tortuosity and curvature, in the susceptibility of atherosclerosis formation. Two works were published about this topic: one

regarding left coronary arteries [2] and another regarding right coronary arteries [3]. Patient-specific coronary arteries, provided by Centro Hospitalar de Vila Nova de Gaia/Espinho (CHVNG/E), with no apparent disease, were used. Equal conditions, such as inlet (Womersley Velocity Profile), outlets (Typical Pressure Profiles) and rheology of blood (Shear-Thinning Model – Carreau Model), were used in order to vary a unique parameter: the geometry of the artery. Despite patients being healthy in the moment of the CT exams, most of them are susceptible for the appearance of atherosclerosis in the future due to the own geometry. When the geometry has drastic curvatures, the tendency to accumulate lipoprotein particles and the tendency to form a stenosis is higher. Deep statistical studies about this theme were performed [2, 3].

The second goal was to compare hemodynamic results considering rigid wall (low computational time in the numerical simulations) and deformable wall (high computational time) [4]. This topic was important to analize if the high computational time considering deformable wall is compensatory, i.e., if the hemodynamic results are significantly different than the ones considering rigid wall. For Computational Fluid Dynamics (CFD), rigid walls, the computational time was 3 hours. Using Fluid-Structure Interaction (FSI), deformable walls, the computational time was 6 days (Intel Core i7-7700K CPU @ 4.20 GHz). Moreover, this study [4] shows that there are not significant differences observed in the time average wall shear stress (TAWSS) in the patient cases (maximum of 2%). Thus, the conclusion was that CFD can be used for hemodynamic simulations since the computational time is lower for further hospital application.

The third goal was to implement the most accurate rheology of blood, the viscoelastic property [5], through the Simplified Phan-Thien/Tanner (sPTT) model. The viscoelastic model predicts peak wall shear stress (WSS) values close to half the magnitude (51%) of Carreau Model, a simplified model [6]. Results were validated from literature indicating very similar approaches [7]. Although the computational time is higher considering sPTT, this model should be used for hemodynamic simulations since it presents more accurate results.

When the R&D Project "PTDC/EMD-EMD/0980/2020 - Coronary Artery Disease Numerical Simulation and Functional Assessment by Advanced Computed Tomography" was funded in March 2021, one of the desired solution is the calculation of the Fractional Flow Reserve (FFR) specific for each patient case [8]. A FFR lower than 0.75 represents a hemodynamically significant stenosis, inducing ischemia and requiring revascularization procedures to the patient. A FFR higher than 0.80 reports a hemodynamically insignificant stenosis. In previous studies, the author and her research team used outlet pressure profiles defined in the literature as typical boundary conditions to model blood flow in arteries [2, 3] and not specific for each patient. The imposition of pressure profiles at the outlet boundaries means a creation of pressure gradient along the artery, which is not physiologically correct and accurate when the distribution of pressure specific for the patient is the desired solution such as the FFR. Thus, the lumped-parameters models (Windkessel models) solve this problem and has been recently implemented by the author and the research team. These models find accurate pressures in the coronary branches based on blood flow resistance. As a proof of concept, the computed FFR using the 3-element Windkessel model was obtained for a patient differing 2.15% the invasive FFR obtained in the hospital [9]; and considering the 5-element Windkessel model differs less than 1% the invasive FFR [10]. Both errors are low.

The final goal of the project is to obtain a non-invasive computed FFR and coronary

hemodynamic descriptors, on-site (in the hospital) and minimizing costs, through a software with the most accurate conditions as possible, assuming pressure profiles specific for each patient artery (Windkessel model) and the most accurate rheology of blood (the viscoelastic property). The validation of the software has started with some patients (work of the present moment), comparing the invasive FFR of the patient, provided by CHVNG/E, with the obtained computed FFR. After validation with many patient-specific cases, the research team will aim to create a software for local use (hospital), allowing a comprehensive assessment of CAD in an accessible, fast, reliable and non-invasive way, as well as cost reduction in the diagnosis and therapeutic guidance of patients with CAD.

2 NUMERICAL IMPLEMENTATION - 2018 TO FEBRUARY 2021

This section reports a review of the numerical implementation regarding the hemodynamic simulations in coronary arteries, since 2018 (when the author became an integrated member of LAETA-INEGI) to February 2021 (before starting the R&D project funded by FCT). The first goal was to correlate the geometric parameters with the atherosustability in left [2] and right patient coronary arteries [3]. The second goal was to compare hemodynamic results considering rigid walls (low computational time) and deformable walls (high computational time) [4]. The third goal was the evaluation of the impact of the most accurate property of blood, the viscoelastic property, in the hemodynamic results [6]. Thus, the following considerations were used and taken into account.

2.1 3D Geometry Construction of the Patient-Specific Coronary Artery

The 3D geometry construction of the patient-specific coronary artery was obtained from Computed Tomography images (Siemens SOMATOM Force®, Erlanger, Germany) provided by the Cardiology Department of CHVNG/E [2-4, 6]. Mimics® and Solidworks® software were used for this construction. In first place, the aorta was selected as well as the coronary artery points of interest such as ostium and multiple side-branches. After segmentation of the coronary path and the lumen area, a 3D mask of the artery was obtained (Fig. 1a). Then, it was necessary to apply a smoothing process to reduce the high roughness of the mask in order to obtain the final 3D geometry (Fig. 1b), which will be used for numerical simulations.

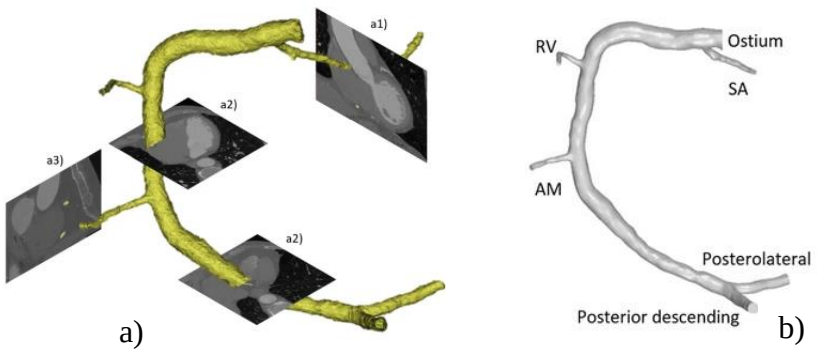

Figure 1: a) Schematic representation of the segmentation process of a coronary artery of a patient. The tri-dimensional mask results from the segmentation of each image slice, from each imaging plane: (a1) coronal; (a2) axial; (a3) sagittal; b) 3D reconstructed model of a patient-specific coronary artery based on CT scans. Adapted from [3].

2.2 3D Mesh Construction of the Patient-Specific Coronary Artery

The 3D mesh construction of the patient-specific coronary artery is achieved using Meshing ANSYS® software. A uniform tetrahedral mesh was built through the Path Independent Method, as can be seen in Fig. 2a. In this way, there is no refinements in unnecessary regions. The study of the accuracy of the mesh combines a lower Maximum Skewness, as possible, and a reasonable computational time.

The Skewness parameter measures the quality and stability of mesh elements. Orthogonality values can oscillate between 0 and 1, so the worst quality elements have an orthogonality close to 1, while the best quality cells have an orthogonality close to 0. The latter tends to be equilateral, angles close to 60 degrees [11]. Thus, the Maximum Skewness value (element with worst quality) must be below 0.90 in order to avoid hindering the solution convergence. For the patient of Fig. 2a, the Maximum Skewness is 0.587 [4].

Furthermore, mesh tests must be performed for the lumen domain. A variable, such as the wall shear stress (WSS), should be represented as a function of the number of mesh elements. The most accurate mesh is the one where the plateau starts - where the WSS does not vary with the number of elements - having the lowest computational time as possible. For the patient case of Fig. 2b, the number of elements that should be used is 400 000 [6].

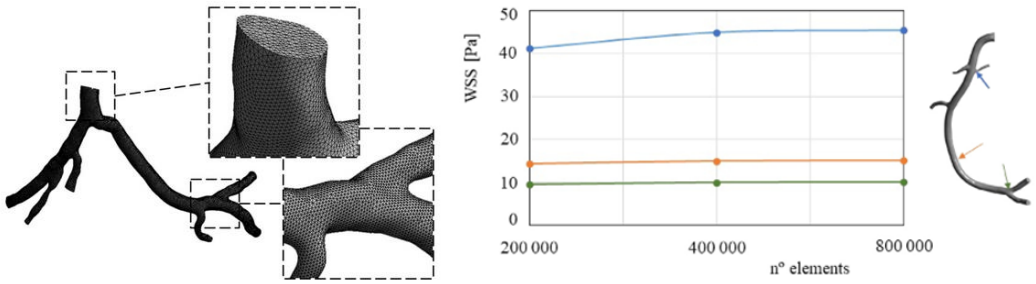

Figure 2: a) Lumen mesh of a coronary artery of a patient. Adapted from [4]; b) WSS in the systolic peak for three tetrahedral meshes considered and for three locations of a patient artery. Adapted from [6].

2.3 Inlet and Outlet Boundary Conditions

The inlet and outlet boundary conditions of the patient cases were imposed in these studies [2-4, 6], since in vivo measured data, concerning the inlet and outlet boundary conditions, were not available at the hospital centre. Mathematical equations were used to simulate the pulsatile nature of blood in each specific artery.

At the inlet, the Womersley velocity profile [12] was considered and implemented in User-Defined Functions (UDF) of ANSYS® software (Fig. 3). This profile is dependent on the time of the cardiac cycle (t) and the position at the inlet (r_d). The Womersley profile adjusts the Poiseuille profile depending on the radius of the vessel (Rd) and the cardiac pulse frequency (ω). Thus, considering blood as an incompressible fluid in a pipe [12, 13], the Womersley velocity is defined by:

$$v(r_d, t) = \frac{A \cdot Rd^2}{i \cdot \mu_f \cdot \alpha^2} \cdot \left(1 - \frac{J_0\left(i^{3/2} \cdot \alpha \cdot \frac{r_d}{Rd}\right)}{J_0\left(i^{3/2} \cdot \alpha\right)}\right) \cdot e^{iwt} \quad (1)$$

i represents the imaginary unit, μ_f the blood viscosity, J_0 the first order Bessel function, $A = \frac{1}{\rho} \cdot \frac{\partial P}{\partial r_d}$ is the pressure gradient, $\alpha = Rd\sqrt{\frac{\rho\omega}{\mu_f}}$ is the Womersley number and ρ the blood density. The Womersley number (α) was calculated for each patient case, based on its equivalent radius (*Rd*) at the inlet (see Table 1).

Table 1: Womersley number specific for each patient radius at the inlet. Adapted from [2].

Number of Patient	**1**	**2**	**3**	**4**	**5**	**6**	**7**	**8**
α	2.93	3.94	3.94	2.84	3.02	3.61	3.51	3.58

At the outlets, the pressure profile is time-dependent but radius-independent (Fig. 3). Since the CT images used to obtain the patient-specific geometries were captured at diastolic phase, the pressure wave (*P(t)*) considered in the computational method was:

$$P(t) = p(t) - p_{diastole} \quad (2)$$

being $p_{diastole}$ equal to 80 mmHg, a value considered to be the normal diastole pressure of a coronary artery [2, 14, 15].

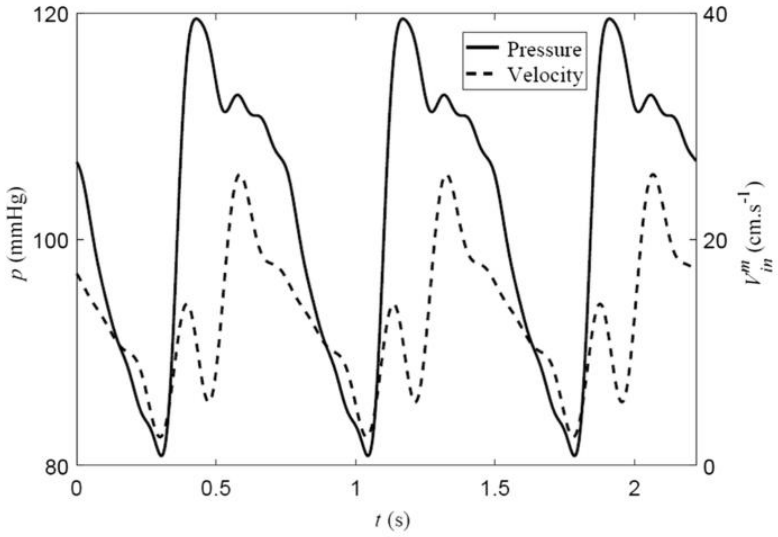

Figure 3: Mean inlet velocity profile and outlet pressure profile along several cardiac cycles. Adapted from [2].

2.4 Implementation of the Fluid-Structure Interaction

Using Fluid-Structure Interaction (FSI) between blood and arterial wall, the mesh of the solid domain (wall of the artery) (Fig. 4b) must be defined beyond the fluid domain (blood) (Fig. 4a).

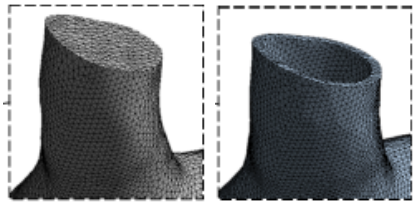

a) b)

Figure 4: a) Mesh of the fluid domain (blood); b) Mesh of the solid domain (wall of the artery). Adapted from [4].

The wall of the coronary artery has characteristics which should be considered in FSI, i.e., in the deformation of the wall according the cardiac cycle. The arterial wall is considered a hyperelastic material - incompressible, isotropic, homogeneous and with constant density (ρ_ω) equal to 1120 kg/m^3. Its stress-strain behaviour is non-linear.

Thus, the Mooney-Rivlin 5-parameter hyperelastic constitutive model was applied [4, 16] taking into account the non-linear incompressibility of arterial wall:

$$W = a_{10}(I_1 - 3) + a_{01}(I_2 - 3) + a_{11}(I_1 - 3)(I_2 - 3) + a_{20}(I_1 - 3)^2 + a_{02}(I_2 - 3)^2 + \frac{1}{d}(J - 1)^2 \quad (3)$$

W represents the deformation energy density function; I_1 and I_2 the first and second stress invariants; d the parameter of incompressibility; J the proportion of elastic volume; and a_{10}, a_{01}, a_{11}, a_{20} and a_{02} the hyperelastic constants that describe the deformation of the material. Therefore, the constants of the model are represented in Table 2.

Table 2: Mooney-Rivlin model constants for the arterial wall. Adapted from [4].

Parameter	Healthy Coronary Artery	Units
a_{10}	-4.020	MPa
a_{01}	4.321	MPa
a_{11}	-51.856	MPa
a_{20}	18.401	MPa
a_{02}	39.105	MPa
d	2.434	MPa^{-1}

Fluid-Structure Interaction (FSI) taking into account deformable walls of the arteries were implemented and used to solve governing equations of the hemodynamics. All the simulations were performed in ANSYS® software [4].

The hemodynamic simulation process using FSI is divided into three steps: pre-processing, solution calculation and post-processing. In pre-processing, the computational mesh of coronary artery, both fluid (blood) and solid (arterial wall), is generated and the boundary conditions and material properties are defined. In solution calculation, the results of the simulations are run in a cyclic process taking into account the coupling mode. In post-processing, the results obtained in the previous step are visualized and analyzed.

Fig. 5 shows the flowchart, clarifying the solution calculation process in a FSI simulation. CFD simulations are simpler. They do not consider the solid domain (arterial wall) and consequently the deformability of the artery (Fig. 6).

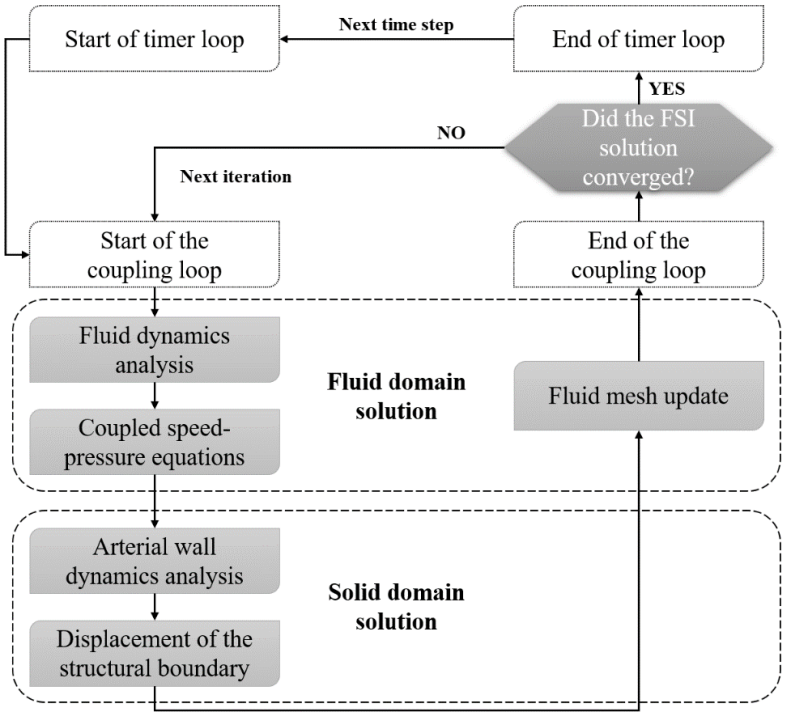

Figure 5: Flowchart to understand FSI simulation process. Adapted from [4].

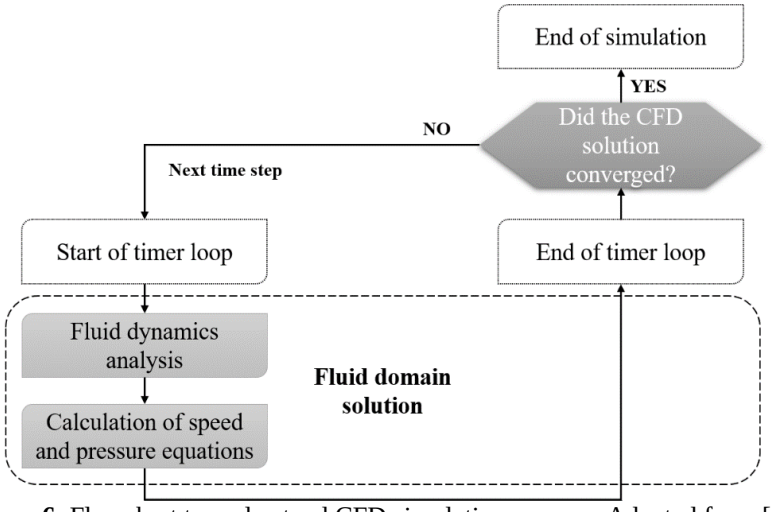

Figure 6: Flowchart to understand CFD simulation process. Adapted from [4].

Looking at Fig. 5, when the fluid domain has been solved and converged, the stress tensor calculated across the fluid domain is transferred to the fluid–structure interface. The solid domain then solves the resulting displacements. Once the solution has converged in the fluid–structure interface, the fluid mesh is updated through a diffusion-based smoothing method [2].

2.5 Implementation of the Accurate Rheology of Blood

Blood is well characterized as an isotropic, incompressible, homogeneous and non-Newtonian fluid, with constant density equal to 1060 kg/m^3. Complex fluids, such as blood, exhibit strange behaviours that depend on underlying structures that form them.

Constitutive models that combine the viscosity part with the elastic part define the viscoelasticity of blood. The extra stress tensor $\boldsymbol{\tau}$ is composed by the sum of the suspending fluid ($\boldsymbol{\tau_s}$) and the elastic ($\boldsymbol{\tau_e}$) contributions:

$$\tau_{ij} = \tau_{ij_s} + \tau_{ij_e} \tag{4}$$

$$\tau_{ijs} = 2\mu_s D_{ij} \tag{5}$$

$$\tau_{ij_e} = \sum_{k=1}^{m} \tau_{ij_k} \tag{6}$$

The subscripts *i* and *j* (Eq. 4) refer to the different Cartesian components, i.e., *x*, *y*, *z*. The solvent contribution (Eq. 5) is associated with the viscous stresses. The elastic stresses (Eq. 6) depends on the viscoelastic model. Eq. 6 shows a multi-mode formulation of the elastic stresses. The total stress component (τ_{ij_e}) is the sum of each *k* mode (τ_{ij_k}) in a total of *m* modes.

$$f(\tau_{ij_k})\tau_{ij_k} + \lambda_k \overset{\nabla}{\tau}_{ij_k} + \alpha_k \frac{\lambda_k}{\mu_{e_k}} \left(\tau_{in_k} \cdot \tau_{nj_k}\right) = 2\mu_{e_k} D_{ij} \tag{7}$$

$$f\left(\tau_{ij_k}\right) = 1 + \frac{\lambda_k \varepsilon_k}{\mu_{e_k}} \, tr\left(\tau_{ij_k}\right) \tag{8}$$

In Equations 7 and 8, μ_{e_k} is the elastic viscosity, λ_k the relaxation time, α_k the mobility factor, ε_k the extensibility coefficient and $\overset{\nabla}{\tau}_{ij_k}$ the upper-convected derivative. These equations are a compact form of representing some viscoelastic models such as the Giesekus and the Simplified Phan-Thien/Tanner (sPTT) models. These constitutive models are different according the existence or non-existence of the mobility factor (α_k) and the extensibility coefficient (ε_k) for each *k* mode (Table 2).

Table 2: Existence and non-existence of mobility factor and extensibility coefficient in Giesekus and sPTT models

Model	$\boldsymbol{\alpha_k}$	$\boldsymbol{\varepsilon_k}$
Giesekus	α_k values	0
sPTT	0	ε_k values

Both Giesekus and sPTT are non-linear models. Numerical solutions considering Giesekus and sPTT have found to be equivalent [6] since according to Campo-Deãno (2013) [5] these models show a similar fit of the viscoelastic property of blood. However, the Giesekus model introduces a non-zero second normal stress difference, which so far has not been reported for blood [5]. Thus, the sPTT model becomes the best option for further applications.

2.5 Numerical Methods

The numerical simulations were performed in ANSYS® software using Fluent and the extensive implementation and use of UDFs.

Regarding FSI and CFD simulations, the values for the lumen domain are the same. For example, considering the time step size equal to 0.005s in a total time of the cardiac cycle 0.74s, the number of time steps is 148 (0.74/0.005) [4]. The difference of using FSI is adding the coupling step, which represents the maximum number of iterations in the structural domain (defined by 30 iterations, for example) for each time step of fluid domain [4]. This maximum number of iterations is necessary to obtain convergence in each coupling step.

Navier-Stokes equations were solved considering the laminar flow of blood and its incompressibility. SIMPLE (Semi-Implicit Method for Pressure Linked Equations) algorithm was used to couple the pressure-velocity equations. Moment equations and equations defining the viscoelastic property, implemented in UDFs [6], were discretized by the second order upwind scheme, while the pressure gradient was discretized according to PRESTO scheme.

3 NUMERICAL IMPLEMENTATION – MARCH 2021 TO CURRENT

This section reports a review of the numerical implementation regarding the hemodynamic simulations in coronary arteries after March 2021 when the R&D Project "PTDC/EMD-EMD/0980/2020 - Coronary Artery Disease Numerical Simulation and Functional Assessment by Advanced Computed Tomography" was funded by FCT in March 2021. The desired solution is the calculation of the Fractional Flow Reserve (FFR) through computational methods, specific for each patient case. The first step to achieve the main goal was the 3D geometry reconstruction of the patient-specific coronary artery in hyperemia conditions, the same conditions used in invasive FFR evaluation, and needed for futher validation. The second step for the goal was the implementation of the lumped-parameters models (Windkessel) for the outlet boundary conditions (pressure). The third step was the FFR calculation through the computed hemodynamic results.

3.1 3D Geometry Construction of Patient Coronary Artery in Hyperemia Conditions

The measurement of the FFR value, invasively, occurs under maximum hyperemia, induced by the intravenous administration of 140μg/kg/min of adenosine in the coronary artery [17]. Due to its administration, a number of physiological changes occur, influencing the estimation of the parameters of the Windkessel models.

The changes are [17]: The heart rate increases by 24bpm; the mean arterial pressure decreases by 6mmHg; the ratio between the resistance (R) in the coronary circulation under maximum hyperemia and under resting conditions is 0.24; the ratio between the cross-sectional area (A) of the coronary artery under maximum hyperemia and under resting conditions is 2.04

(Eq. 9); the velocity at the inlet to the coronary artery is increased by a factor of 2.16 and produce an increase in blood flow by a factor of 4.4.

$$\frac{R_{hyperemia}}{R_{resting}} = 0.24 \Leftrightarrow \frac{r_{resting}^4}{r_{hyperemia}^4} = 0.24 \Leftrightarrow \frac{A_{hyperemia}}{A_{resting}} = 2.04 \quad (9)$$

The model for a patient coronary artery under resting conditions was obtained from the CT images by using the Mimics® software. Then, this model was scaled by a factor of 2.04 to obtain the patient coronary artery under maximum hyperemia, using Mimics® and 3-matic® software [18].

Mimics® software allowed the semi-automatic reconstruction of the lumen of the coronary artery. The aorta and multiple points along the coronary geometry were selected for the reconstruction of the coronary artery with stenosis (see example of Fig. 7).

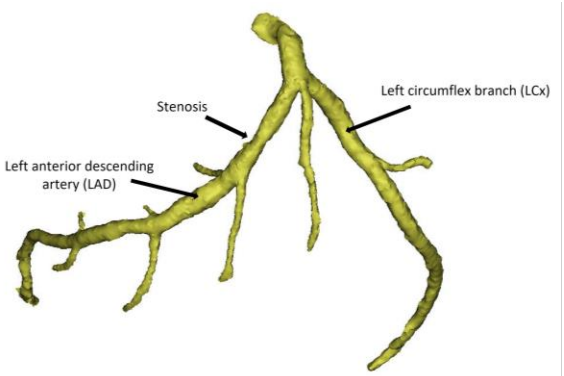

Figure 7: 3D reconstructed model of the coronary artery using Mimics®. Adapted from [18].

However, the model still needs to be smoothed since it has very high roughness. Furthermore, the inlets and outlets need to be defined to run the hemodynamic simulations in ANSYS Fluent®. These changes were done in the 3-matic® software using smoothing and trimming tools (Fig. 8).

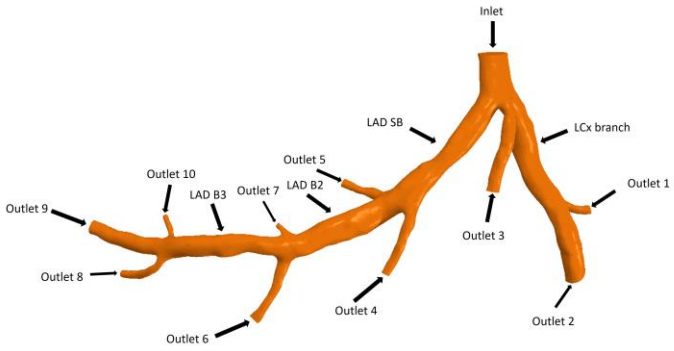

Figure 8: Model of the patient coronary artery under resting conditions. Adapted from [18].

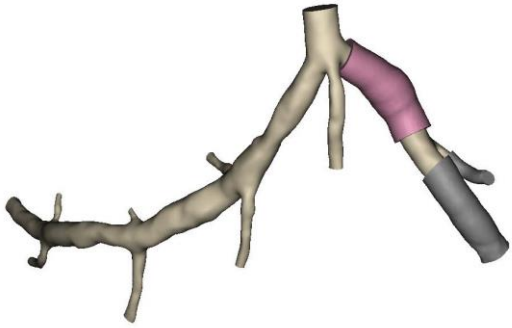

Figure 9: Scaled branches of the coronary artery. Adapted from [18].

Afterwards, the scaled branches were constructed and connected at the intersections between different branches, using the loft feature, the push and pull command, as well as smoothing tools (Fig. 9). The comparison, through overlapping, between the coronary artery model under resting and hyperemic conditions, is represented in Fig. 10. The final model for the patient coronary artery under maximum hyperemia is represented in Fig. 11 [18].

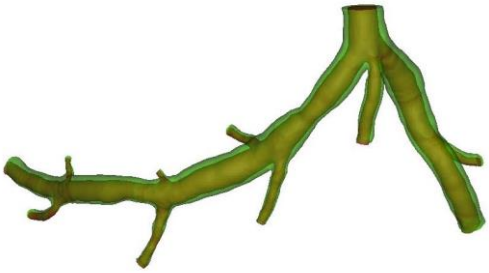

Figure 10: Overlapping representation of the patient coronary artery under resting and hyperemic conditions. Adapted from [18].

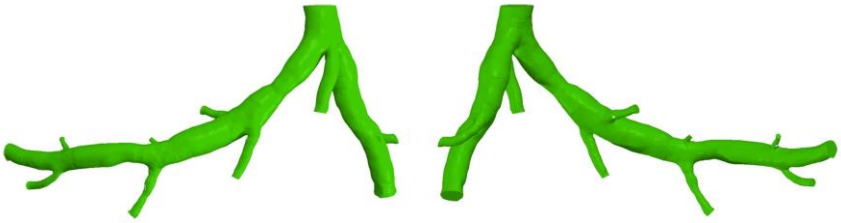

Figure 11: Geometric model of the patient coronary artery under hyperemic conditions. Adapted from [18].

3.2 Implementation of the Windkessel models for Outlet Boundary Conditions

For the outlet boundary conditions, 3-element and 5-element Windkessel models were implemented in UDFs in ANSYS Fluent® software in order to analyze the hemodynamic result differences considering both models. The Windkessel models are important to use since the real pressure inside a patient coronary artery is the desired solution. The models can give the real

hemodynamic solution of a patient.

The Windkessel models make use of an analogy with electrical circuits, with no issues, since the theory of electrical circuits is well developed.

3-element Windkessel model

The 3-element Windkessel model as a coronary artery outlet boundary condition is represented in Fig. 12.

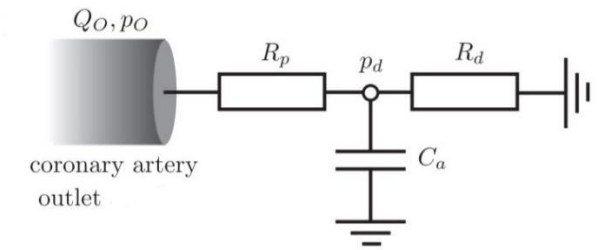

Figure 12: The 3-element Windkessel model as a coronary artery outlet boundary condition. Adapted from [19].

This model is composed by two resistances and one compliance. R_p represents the proximal resistance of the vasculature downstream of the vessel where the boundary condition is applied. R_d represents the distal resistance and C_a the compliance of the downstream vessels. Q_o and p_o represent the volume flow rate and the pressure, respectively, at the outlet at which this boundary condition is applied. p_d represents the pressure at the arteriolar and capillary level.

Eq. 10 represents the governing equations of the 3-element Windkessel model:

$$\frac{d(p_o - R_p Q_o)}{dt} + \frac{1}{C_a R_d}(p_o - R_p Q_o) = \frac{1}{C_a} Q_o \tag{10}$$

This equation was discretized using a second-order implicit scheme, accordingly to the ANSYS Fluent Theory Guide [20]:

$$p_o^{i+1} = \frac{Q_o^{i+1} + \frac{R_p C_a}{\Delta t}\left(\frac{3}{2}Q_o^{i+1} - 2Q_o^{i} + \frac{1}{2}Q_o^{i-1}\right) + \frac{C_a}{\Delta t}\left(2p_o^{i} - \frac{1}{2}p_o^{i-1}\right) + \frac{R_p}{R_d}Q_o^{i+1}}{\frac{3C_a}{2\Delta t} + \frac{1}{R_d}} \tag{11}$$

The superscript i indicates the value of the variable at the current time step, $i+1$ indicates the value of the corresponding variable at the next time step, and $i-1$ indicates the respective value at the previous time step. Δt is the time step chosen for the hemodynamic simulations. The values of R_p, R_d and C_a, for each outlet, are well defined in the literature [19, 21]

The total coronary resistance (R_{tot}) needs to be divided by the outlets of the patient coronary model, accordingly to the area of each outlet. The resistance for outlet i of area A_i is given by the following equation:

$$R_i = R_{tot} \frac{\sum_{i=1}^{n} A_i}{A_i} \tag{12}$$

where the total resistance, R_{tot}, for the coronary tree is given by Eq. 13 and P_{avg} is the average pressure along the cardiac cycle and Q_{avg} the average volume flow rate. The average pressure was calculated using Eq. 14 where $P_{systolic}$ and $P_{diastolic}$ are the systolic and diastolic pressures, respectively.

$$R_{tot} = \frac{P_{avg}}{Q_{avg}} \tag{13}$$

$$P_{avg} = \frac{P_{systolic} + 2P_{diastolic}}{3} \tag{14}$$

The total compliance of the downstream vessels, C_a, is determined by Eq. 15 where P_{es} represents the end-systolic pressure.

$$P_{diastolic}(t) = P_{es} e^{-t/RC_a} \tag{15}$$

The compliance of each outlet is determined by the same way of the resistance, i.e., according to each outlet's area:

$$C_i = C_a \frac{A_i}{\sum_{i=1}^{n} A_i} \tag{16}$$

5-element Windkessel model

The 5-element Windkessel model as a coronary artery outlet boundary condition is represented in Fig. 13 and is more complex than the 3-element model.

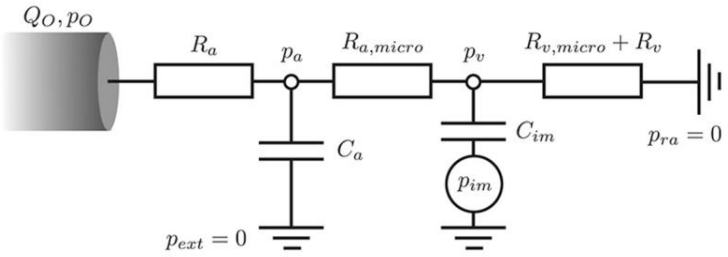

Figure 13: The 5-element Windkessel model as a coronary artery outlet boundary condition. Adapted from [19].

This model is composed by R_a, R_v, $R_{a,micro}$ and $R_{v,micro}$ representing the resistance of the arterial, venous and both arterial and venous capillary levels, respectively. C_a and C_{im} are the arterial and intramyocardial compliances, and p_a, p_v and p_{im} correspond to the arterial, venous and variable intramyocardial pressures, respectively [19]. Moreover, the external pressure, p_{ext}, and the heart's right atrium pressure, p_{ra}, are considered null. The 5-element Windkessel model is defined by the following equations:

$$p_0 = p_a + R_a Q_0 \tag{17}$$

$$\frac{dp_a}{dt} = \frac{Q_0}{C_a} - \frac{p_a - p_v}{C_a R_{a,micro}} \tag{18}$$

$$\frac{dp_v}{dt} = \frac{dp_{im}}{dt} + \frac{1}{C_{im}}\left(\frac{p_a - p_v}{R_{a,micro}} + \frac{p_v}{R_{v,micro} + R_v}\right) \tag{19}$$

The involved parameters are calculated based on patient data but other considerations were necessary. In the systolic phase, the intramyocardial pressure was considered equal to the left ventricular pressure, the pressure at the inlet of the coronary artery. The transition between systole and diastole was neglected and the pressure during the diastole was considered null. The total resistance to flow, R_{total}, involving arterial and venous circulation, was determined by:

$$R_{total} = \frac{\frac{P_{systolic} + 2P_{diastolic}}{3}}{\bar{Q}_i} \tag{20}$$

where $\bar{Q}_i$ is the average flow rate in the inlet. The resistance to blood flow in each outlet, R_i, is determined in the same manner of the 3-element Windkessel model (Eq. 12) and the micro-circulatory arterial resistance, R_m, is given by:

$$R_m = R_{a,micro} + R_a \tag{21}$$

The resistance in the venous circulation, the sum of R_v and $R_{v,\,micro}$, was obtained considering that the average pressure in the veins is equal to 2666.45 Pa [22]:

$$R_{v_i} + R_{v,micro_i} = 2666.45\ \frac{A_i}{\sum_{i=1}^{N} A_i}. \tag{22}$$

The arterial resistance (R_{a_i}) can be determined by:

$$R_{a_i} = \frac{\rho\sqrt{\frac{2}{3\rho}(k_1 \cdot e^{k_2 Rd_i} + k_3)}}{A_i} \tag{23}$$

where ρ of blood is considered constant and equal to 1060 kg m^{-3}, Rd_i is the radius of the outlet and the constants k_1, k_2 and k_3 are equal to 2000 kg^2 s^{-1} m^{-1}, -2253 m^{-1} and 86.5 kg^2 s^{-1} m^{-1}, respectively [22].

Then, the arterial microcirculation resistance ($R_{a,micro_i}$) can be obtained through:

$$R_{a,micro_i} = R_{total} - \left(R_{v_i} + R_{v,micro_i}\right) - R_{a_i} \tag{24}$$

Thus, the resistances of each outlet of the patient are calculated. The values of the total arterial and intramyocardial capacitances, $C_{a,tot}$ and $C_{im,tot}$, are 1.998×10^{-10} m^3 Pa^{-1} and 3.904×10^{-9} m^3 Pa^{-1}, respectively [22]. The authors assume that the myocardium mass of this patient is 204.9 g based on the works of the analysis of male cadaveric hearts [23], since there are no works in literature which measure the myocardial mass of ischemic live patients.

Like the 3-element Windkessel model, the 5-element model was programmed in C language in UDFs of ANSYS Fluent® software. The equations were also discretized using a second-order implicit scheme, following the ANSYS Fluent Theory Guide [24]:

$$\frac{dq}{dt} = \frac{3Q_0^{i+1} - 4Q_0^i + Q_0^{i-1}}{2\Delta t} \tag{25}$$

$$\frac{dp_{im}}{dt} = \frac{3p_{im}^{i+1} - 4p_{im}^i + p_{im}^{i-1}}{2\Delta t} \tag{26}$$

$$aux = \frac{3C_m}{2\Delta t} + \frac{1}{R_m} + \frac{1}{R_{v,micro} + R_v} \tag{27}$$

$$p_0^{i+1} = \frac{\left(1 + \frac{R_a}{R_m}\right) Q_0^{i+1} + C_a \left(R_a dq - \frac{-4p_0^i + p_0^{i-1}}{2\Delta t}\right)}{\frac{3C_a}{2\Delta t} + \frac{1}{R_m} - \frac{1}{aux\, R_m^2}} \tag{28}$$

$$p_v^{i+1} = \frac{1}{aux}\left(\frac{p_0^{i+1}}{R_m} + C_m\left(dp_{im} - \frac{-4p_v^i + p_v^{i-1}}{2\Delta t}\right) - \frac{R_a}{R_m} Q_0^{i+1} + \frac{p_{ra}}{R_{v,micro} + R_v}\right) \tag{29}$$

3.3 Calculation of the Fractional Flow Reserve

After implementing the UDFs referred previously and running hemodynamic simulations in ANSYS® software, the FFR is calculated by:

$$FFR = \frac{p_d}{p_a} \tag{30}$$

p_d is the distal pressure, measured 20mm after the centre of the stenosis. p_a is the aortic pressure, measured at a distance of approximately 10mm from the entrance of the coronary artery [25, 26]. Both p_d and p_a are average pressures (p_{avg}) along the cardiac cycle:

$$p_{avg} = \frac{1}{T}\int_0^T P dt \tag{31}$$

T is the time of the cardiac cycle and *P* is the pressure value of each time instant. The locations of the distal and the aortic planes, where the pressures are measured both invasively (in the hospital) and computationally, are represented in Fig. 14.

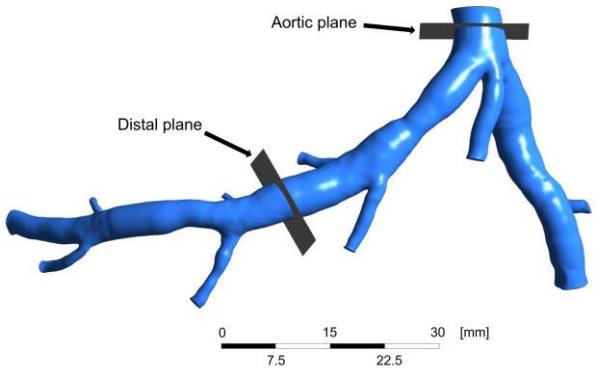

Figure 14: Location of the aortic plane and the distal plane. Adapted from [18].

A FFR value lower than 0.75 represents a hemodynamically significant stenosis, inducing ischemia and requiring revascularization procedures. However, a FFR value higher than 0.80 represents a hemodynamically insignificant stenosis, not inducing ischemia and not requiring revascularization. For FFR values between 0.75 and 0.80, the decision to follow through on revascularization lies with the clinician and their understanding whether it is beneficial or not [26].

Thus, a proof of concept study has already been performed and published in scientific papers [9, 10]. The calculated FFR was compared with the invasive FFR measured for a patient case in the hospital. The computational time considering CFD, the viscoelastic property of blood (sPTT) and both 3 and 5-element Windkessel models was 1:30h (Workstation Desktop Intel Core i9 Extreme Processor units 4 × 3.0 GHz and 64 GB RAM). The calculated FFR value considering the 3-element model (FFR_{comp}=0.910) presents an error of only 2.15% relative to the invasive FFR (FFR_{inv}=0.93). The calculated FFR taking into account the 5-element model (FFR_{comp}=0.925) presents an error of only 0.53% comparing to the invasive FFR. Since the computational time is the same and the relative error is lower for both models, the 3-element Windkessel model can be used since it is simpler and requires less estimated parameters then the 5-element model.

4 FINAL REMARKS AND FUTURE DIRECTIONS

This study reports a review of the numerical implementation of the author and her research team for hemodynamic simulations in patient-specific coronary arteries. The author highlights her two lines of research since she is an Integrated Member of the Institute of Science and Innovation in Mechanical and Industrial Engineering (LAETA-INEGI), since 2018.

One line of research was from 2018 (when the author became an integrated member of LAETA-INEGI) to February 2021 (before starting the R&D project funded by FCT). At this time, the first goal was to correlate the geometric parameters with the tendency to form

atherosclerosis in left [2] and right patient coronary arteries [3]. The second goal was comparing hemodynamic results considering rigid walls, where the computational time is low, and deformable walls where the computational time is high [4]. The third goal was the assessment of the impact of the most accurate property of blood, the viscoelastic property, in the hemodynamic results [6]. Thus, the following tasks were used and taken into account in this part of the work: (1) 3D reconstruction of the patient-specific coronary artery, (2) 3D mesh construction of the patient-specific coronary artery, (3) Implementation of the Womersley velocity profile at the inlet, (4) Implementation of the pressure profile at the outlet based on the literature, (5) Implementation of the Fluid-Structured Interaction (FSI) between blood and wall, (6) Implementation of the most accurate rheology of blood, the viscoelastic property.

After implementations in UDFs and running the hemodynamic simulations, the main conclusions were: (1) The atherosusceptibility depends on the curvature and tortuosity of the artery [2, 3]; (2) CFD can be used since the computational time is substantially lower than FSI and results have a difference of 2% in the maximum [4]; (3) The viscoelastic model for blood, sPTT, should be used since it is the most accurate [6].

Taking into account the previous conclusions, the author constructed another line of research in March 2021 when she won, as Principal Investigator (PI), the financial support of the Foundation for Science and Technology Portugal (FCT) regarding the R&D Project "PTDC/EMD-EMD/0980/2020. In this project, the desired solution is the calculation of the Fractional Flow Reserve (FFR) through computational methods, specific for each patient case. The first step to achieve the main goal was the 3D geometry reconstruction of the patient-specific coronary artery in hyperemia conditions - the same conditions which the invasive FFR was measured in the hospital for futher validation. The second step for the goal was the implementation of the lumped-parameters models (Windkessel) for the pressure boundary conditions at the outlets. The third step was the FFR calculation through the computed hemodynamic results and comparing them with the invasive FFR.

The novelty of this part of work is considering two properties simultaneously - viscoelastic property of blood and Windkessel model for outlet boundary conditions - where no authors, as far as we know, have considered in the literature. Thus, after these three steps, the main conclusion was: Since the computational time is the same and the relative error is low for both models (2.15% for 3-element and 0.53% for 5-element), the 3-element Windkessel model can be used for hemodynamic simulations [9, 10]. It is a simpler model and requires less estimated parameters than the 5-element. Consequently the 3-element model is less susceptible to errors.

The study cited previously is a proof of concept with only one patient case, needing future directions. Thus, the validation, comparing the computed FFR with the invasive FFR, must be done for many patient-specific cases with atherosclerotic disease with different degrees of stenosis and different locations. Moreover, a Python software has been developed for automatic construction of the coronary arteries since it is faster and less costly than manual construction through commercial software.

ACKNOWLEDGMENTS

The author gratefully acknowledge the financial support of the Foundation for Science and Technology (FCT) of Portugal regarding the R&D Project "CADS-FACT – PTDC/EMD-

EMD/0980/2020", the Engineering Faculty of the University of Porto (FEUP), the Institute of Science and Innovation in Mechanical and Industrial Engineering (INEGI), the Cardiovascular R&D Unit of the Faculty of Medicine of the University of Porto (FMUP) and the Cardiology Department of the Vila Nova de Gaia/Espinho Hospital Centre (CHVNG/E). Moreover, an acknowledgment to the Transport Phenomena Research Center (CEFT) where the author started the basis of Cardiovascular Engineering during her Post-Doctoral in Mechanical Engineering from 2012 to 2017.

REFERENCES

[1] Mozaffarian, D., Benjamin, E.J., Go, A.S. et al. 2016. "Heart disease and stroke statistics – 2016 update." Circulation 131: e38-360.

[2] Pinho, N., Castro, C.F., António, C.C., Bettencourt, N., Sousa, L.C., Pinto, S.I.S. 2019. "Correlation between geometric parameters on the left coronary artery and hemodynamic descriptors of atherosclerosis: FSI and statistical study." Medical & Biological Engineering & Computing 57: 715-729. https://doi.org/10.1007/s11517-018-1904-2

[3] Pinho, N., Sousa, L.C., Castro, C.F., António, C.C., Carvalho, C., Ferreira, W., Ladeiras-Lopes, R., Ferreira, N.D., Braga, P., Bettencourt, N., Pinto, S.I.S. 2019. "The impact of the right coronary artery geometric parameters on hemodynamic performance." Cardiovascular Engineering and Technology 10: 257-270. https://doi.org/10.1007/s13239-019-00403-8

[4] Miranda, E., Sousa, L.C., António, C.C., Castro, C.F., Pinto, S.I.S. 2021. "Role of the left coronary artery geometry configuration in atherosusceptibility: CFD simulations considering sPTT model for blood." Computer Methods in Biomechanics and Biomedical Engineering 24: 1488-1503. https://doi.org/10.1080/10255842.2021.1894555

[5] Campo-Deaño L., Dullens R.P.A., Aarts D.G.A.L., Pinho F.T., Oliveira M.S.N. 2013. "Viscoelasticity of blood and viscoelastic blood analogues for use in polydymethylsiloxane in vitro models of the circulatory system." Biomicrofluidics 7: 34102. https://doi.org/10.1063/1.4804649

[6] Pinto, S.I.S., Romano, E., António, C.C., Sousa, L.C., Castro, C.F. 2020. "The impact of non-linear viscoelastic property of blood in right coronary arteries hemodynamics – a numerical implementation." International Journal of Non-Linear Mechanics 123: 103477. https://doi.org/10.1016/j.ijnonlinmec.2020.103477

[7] Good, B.C., Deutsch, S., Manning, K.B. 2016. "Hemodynamics in a pediatric ascending aorta using a viscoelastic pediatric blood model." Ann. Biomed. Eng. 44: 1019-1035. https://doi.org/10.1007/s10439-015-1370-z

[8] Nagel, E., Greenwood, J.P., McCann, G.P., Bettencourt, N., et al. 2019. "Magnetic

Resonance Perfusion or Fractional Flow Reserve in Coronary Disease." N Engl J Med 380: 2418-2428. https://doi.org/10.1056/NEJMoa1716734

[9] Fernandes, M., Sousa, L.C., António, C.C., Pinto, S.I.S. 2024. "Accuracy and temporal analysis of non-Newtonian models of blood in the computational FFR – Numerical implementation.", International Journal of Non-Linear Mechanics 161: 104683. https://doi.org/10.1016/j.ijnonlinmec.2024.104683

[10] Fernandes, M., Sousa, L.C., António, C.C., Pinto, S.I.S. 2023. "Modeling the Five-Element Windkessel Model with Simultaneous Utilization of Blood Viscoelastic Properties for FFR Achievement: A Proof-of-Concept Study.", Mathematics 11: 4877. https://doi.org/10.3390/math11244877

[11] ANSYS. 2009. 6.2.2 Mesh Quality. ANSYS FLUENT 120 User's Guid.

[12] Womersley, J.R. 1955. "Method for the calculation of velocity, rate of flow and viscous drag in arteries when the pressure gradient is known." J Physiol 127: 553–563. https://doi.org/10.1113/jphysiol.1955.sp005276

[13] Sousa, L.C., Castro, C.F., António, C.C. et al. 2014. "Toward hemodynamic diagnosis of carotid artery stenosis based on ultrasound image data and computational modeling." Med Biol Eng Comput 52: 971–983. https://doi.org/10.1007/s11517-014-1197-z

[14] Park, C.G., Lee, J.Y. 2011. "The significance of the J-curve in hypertension and coronary artery diseases." Korean Circ J 41: 349–353. https://doi.org/10.4070/kcj.2011.41.7.349

[15] Torii, R., Wood, N.B., Hadjiloizou, N. et al. 2009. "Fluid–structure interaction analysis of a patient-specific right coronary artery with physiological velocity and pressure waveforms." Commun Numer Methods Eng 25: 565–580. https://doi.org/10.1002/cnm.1231

[16] Karimi, A., Navidbakhsh, M., Shojaei, A., Hassani, K., Faghihi, S. 2014. "Study of plaque vulnerability in coronary artery using Mooney-Rivlin model: a combination of finite element and experimental method." Biomed Eng – Appl Basis Commun 26: 1450013. https://doi.org/10.4015/S1016237214500136

[17] Wilson, R.F., Wyche, K., Christensen, B.V., Zimmer, S., Laxson, D.D. 1990. "Effects of adenosine on human coronary arterial circulation." Circulation 82: 1595-1606. https://doi.org/10.1161/01.CIR.82.5.1595

[18] Martins, A.A., Castro, C.F., António, C.C., Sousa, L.C., Pinto, S.I.S. 2023. "FFR quantification in a left coronary artery using a three-element Windkessel model and the non-linear viscoelastic property of blood." Mathematics and Mechanics of Complex Systems 11: 349-379. https://doi.org/10.2140/memocs.2023.11.349

[19] Jonášová, A., Vimmr, J. 2021. "On the relevance of boundary conditions and viscosity models in blood flow simulations in patient-specific aorto-coronary bypass models." International Journal for Numerical Methods in Biomedical Engineering 37: e3439. https://doi.org/10.1002/cnm.3439

[20] ANSYS, Inc., "Temporal discretization," January 2009. [Online]. Available: https://www.afs.enea.it/project/neptunius/docs/fluent/html/th/node367.htm. [Accessed 07 September 2022].

[21] Deyranlou, A., Naish, J.H., Miller, C.A., Revell, A., 2020. "Numerical study of atrial fibrillation effects on flow distribution in aortic circulation." Annals of biomedical engineering 48: 1291–1308. https://doi.org/10.1007/s10439-020-02448-6

[22] Boileau, E., Pant, S., Roobottom, C., Sazonov, I., Deng, J., Xie, X., Nithiarasu, P. 2018. "Estimating the Accuracy of a Reduced-order Model for the Calculation of Fractional Flow Reserve (FFR)." Int. j. numer. method. biomed. eng. 34: e2908. https://doi.org/10.1002/cnm.2908

[23] Dadgar, S.K., Tyagi, S.P. 1979. "Importance of Heart Weight, Weights of Cardiac Ventricles and Left Ventricle Plus Septum/Right Ventricle Ratio in Assessing Cardiac Hypertrophy." Jpn. Heart J. 20: 63–73. https://doi.org/10.1536/ihj.20.63

[24] Inc., A. Temporal Discretization Available online: https://www.afs.enea.it/project/neptunius/docs/fluent/html/th/node367.htm (accessed on 4 April 2021).

[25] Lerman, A., Li, J. 2017. "Fractional Flow Reserve," [Online]. Available: https://www.thecardiologyadvisor.com/home/decision-support-in-medicine/cardiology/fractional-flow-reserve/. [Accessed 15 March 2022].

[26] Chahour, K., Aboulaich, R., Habbal, A., Zemzemi N., Abdelkhirane, C. 2020. "Virtual FFR Quantified with a Generalized Flow Model Using Windkessel Boundary Conditions." Computational and mathematical methods in medicine 2020: 3942152. https://doi.org/10.1155/2020/3942152